

Extraplanar gas in Edge-on Galaxies traced by SOFIA observations of [C II]

WILLIAM T. REACH,¹ DARIO FADDA,¹ RICHARD J. RAND,² GORDON J. STACEY,³

¹*Universities Space Research Association, MS 232-11, Moffett Field, CA 94035, USA*

²*Department of Physics and Astronomy, University of New Mexico, 800 Yale Blvd, NE, Albuquerque, NM 87131, USA*

³*Astronomy Department, Cornell University, Ithaca, NY 14853*

ABSTRACT

Bursts of localized star formation in galaxies can levitate material from the midplane. Spiral galaxies that are edge-on allow clear distinction of material that is levitated off the galaxies midplanes. We used SOFIA to measure the vertical distribution of [C II] 157.7 μm line emission for two nearby, edge-on galaxies, NGC 891 and NGC 5907. We find that for the central region and actively-star-forming regions in the northern portion of NGC 891, and for NGC 5907, a thin (0.3 kpc) disk is supplemented by a thick disk with an exponential scale height of ~ 2 kpc. The [C II] is far more extended than mid-infrared emission (0.1 kpc, tracing present-day massive star formation) but not as extended as the H I (100 kpc, tracing low-metallicity circum/inter-galactic matter). The extraplanar [C II] may arise in walls of chimneys that connect the disk to the halo.

1. INTRODUCTION

The vertical distribution of material in disk galaxies is determined by a balance between gravity from the stellar disk and pressure (thermal, magnetic, relativistic particles) in the interstellar gas. In the Milky Way, cloud pressures and density of starlight can be measured locally, but without large-scale context due to our location within the disk. In particular, material far from the midplane of the galaxy is difficult to separate from local gas. Active star formation in the midplane of a galaxy, and collisions with other galaxies, can increase the thickness of disks, with stars (collisionless) and gas (collisional) responding differently. Bursts of localized star formation can form large-scale bubbles (Heiles 1990; Breitschwerdt & de Avillez 2006) or drive material into the halo as ‘worms’ (Heiles et al. 1996), whence it returns to the midplane as a ‘galactic fountain’ (Bregman 1980; Norman & Ikeuchi 1989) or if sufficiently powerful escapes as a wind (Heckman et al. 1990).

Edge-on galaxies offer a prime opportunity to measure the vertical distribution of both stars and interstellar material. For a galaxy that is exactly edge on, the angular distance from the ridge of peak brightness is readily interpreted as vertical displacement from the galactic midplane. There are several well-known, nearby, nearly edge-on galaxies, which exhibit distinct, dramatic dust lanes due to absorption of starlight by dust along a long path length through the disk. If a galaxy is inclined by at least 87° and is comparable in size to the Milky Way, then the thin disk can be separated from potentially thicker distribution of ‘extraplanar’ gas. Fortunately, nature provides several such nearby, nearly-edge-on galaxies. Extraplanar gas extending to 5 kpc was detected in H α observations of the nearly edge-on galaxy NGC 891 (Rand 1997), and even 13 kpc above NGC 5775 (Boettcher et al. 2019; Rand 2000) requiring processes both to levitate the material and keep it ionized. In another edge-on galaxy, NGC 5907, deep optical images revealed streams interpreted as the ‘ghost’ of dwarf galaxy collisions during formation (Martínez-Delgado et al. 2008), although that galaxy shows no evidence for extraplanar diffuse ionized gas (Rand 1996).

The scale height of the ISM in the Milky Way was measured from [C II] observations with *Herschel* Langer et al. (2014), with a FWHM of 172 pc, intermediate between molecular gas traced by CO (110 pc) and atomic gas traced

wreach@sofia.usra.edu

dfadda@sofia.usra.edu

rjr@umn.edu

stacey@astro.cornell.edu

by H I (230 pc). [C II] emission can be produced by a wide range of interstellar gas, including ionized, atomic, and molecular. It is the most intense spectral line from many galaxies and dominates the cooling for atomic and diffuse molecular gas. High-latitude clouds evidently contain a significant fraction of ‘dark gas, which is likely predominantly H₂ but without discernible emission from detectable tracers like CO. The amount of such ‘dark gas was measured independently using gamma-rays as a total nucleon tracer (via the interaction between cosmic rays and interstellar protons (Grenier et al. 2005) and far-infrared dust emission (Heiles et al. 1988; Reach et al. 2015; Leroy et al. 2011) as total column density tracers. ‘Dark gas appears to be of order 40% of the total molecular gas mas in the local Milky Way. That same proportion is unlikely to apply in all galaxies nor at all galactocentric radii nor distances from the midplane. Far-infrared observations of [C II] can explore the presence of ‘dark gas in galaxy halos.

Nearby galaxies provide the bridge between the Milky Way and distant galaxies, and nearby, edge-on galaxies provide the best access to the vertical distribution and the connection between galaxies’ disks and halos. For distant galaxies, [C II] is one of the few spectral lines that can be used as a signpost for star formation, and a measure of local far-UV radiation field strength, hence star formation intensity (Stacey et al. 1991; Pineda et al. 2018). In edge-on galaxies, extraplanar, diffuse ionized gas, traced by H α , is more prominent with higher SFR surface density (e.g. Rand 1996; Rossa & Dettmar 2003), as is extraplanar dust absorption (Howk & Savage 1999). The H α plumes extended from the midplane are possible chimneys where material that has been heated and accelerated by active star formation regions vents into the halo. For the best-studied edge-on galaxy, NGC 891, the H I distribution is very extended, with a thin disk of exponential scale height of 0.2 kpc and an extended distribution with approximate scale height of 2.5 kpc (Oosterloo et al. 2007). In a more face-on galaxy, NGC 6946, the H I distribution reveals in-falling gas that may lead to holes in midplane (Boomsma et al. 2008), so the extended extraplanar gas can not only be the up-welling exhaust of chimneys from massive stars but also the returning gas. Extraplanar H I was found to have a global infall rate of $\sim 25 \text{ km s}^{-1}$, which could be the incoming part of galactic fountain (Heald et al. 2011; Marasco et al. 2019). A thick disk with scale height 1.4 kpc was detected in far-infrared dust observations of NGC 891 (Bocchio et al. 2016). Another component of galaxies, relativistic particles, has an extended scale height, measured at 1.3 kpc for the disk of NGC 891 (Schmidt et al. 2019). In [C II], there was a hint of an extended disk already in the NGC 891 *Herschel* observations with a measured scale height of 300 pc for the inner 3 kpc radial distance that was observed (Hughes et al. 2015).

In this paper we address the [C II] distribution, tracing the disk-halo connection, for two prominent, nearby, edge-on galaxies NGC 891 and NGC 5907, to measure the vertical distribution of a tracer of higher-density material than is traced by H α , H I, or cosmic rays.

2. OBSERVATIONS

The observations were part of SOFIA Cycle 6 observing program 06_0010. The Field Imaging Far-Infrared Line Spectrometer (FIFI-LS; Fischer et al. (2018)) was used to map the vertical extents of NGC 891 and NGC 5907 in the [C II] 157.741 μm (rest frame) line. The spectral resolving power of FIFI-LS in the [C II] line is 1200, corresponding to velocity resolution 250 km s^{-1} . Because FIFI-LS is a dual-channel instrument, we simultaneously observed the [O III] 88.356 μm line; the signal-to-noise was not sufficient in that line, so those data will not be discussed in this paper. Table 1 shows the SOFIA observation conditions, which were conducted using 5.8 hr of flight time.

Figure 1 shows the regions that were imaged: two fields, NGC 891-North and NGC 891-South, cover a range of longitudes along the midplane and 3 kpc vertical extend from the midplane of that galaxy, and one field covers the central longitudes of NGC 5907. The observations were performed with the secondary mirror chopping between the galaxy and a reference field, which alternated between fields on either side of the galaxy 300'' from the midplane. The instantaneous field of view was 60'' \times 60'' with 5 \times 5 spaxels of 12'' \times 12'' each. The total field we covered comprise a set of dithered raster pointings that span a large portion of the galaxy while filling in the gaps between spaxels, which allows for drizzling onto a fine, well-sampled grid during data reduction. The data were processed into data cubes (RA, Dec, Velocity) by the SOFIA science center including drizzling onto a fine grids of 5'' sampling. At the distances of NGC 891 and NGC 5907, the pixel sizes are 190 pc and 370 pc, respectively.

To improve the separation between the thin, bright emission from the midplane and the extended, faint emission of the extraplanar gas, we reprocessed the data using a narrower spatial kernel. Whereas the standard data processing uses a spatial window of 2 \times the beam and a wavelength kernel of 1.2 \times the spectral resolution. We reprocessed using a spatial window of 1 \times the beam and a wavelength kernel of 0.5 \times the spectral resolution. This processing more closely matches that of *Herschel*/PACS, aiding inter-comparison.

Table 1. SOFIA Observing Log

Target	Date	Flight	Altitude (feet)	Elevation (°)	Exposure (min)
NGC 891-South	2019 Feb 28	549	38,500	47	34
NGC 5907	2019 Mar 02	551	42,800	45	32
NGC 891-North	2019 Nov 05	635	44,380	49	17
NGC 891-North	2019 Nov 08	638	42,280	53	22
NGC 891-North	2019 Nov 13	639	45,890	52	16

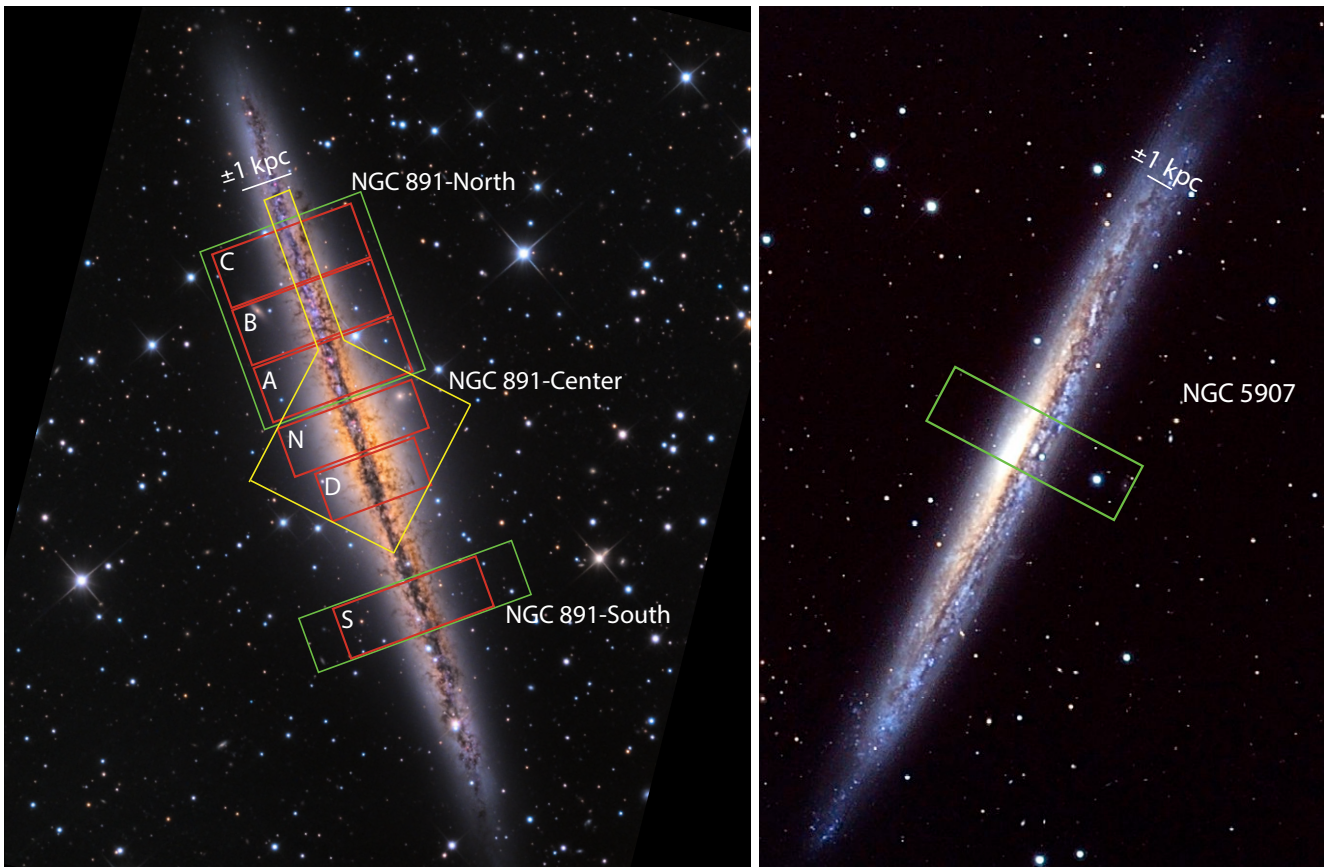


Figure 1. Overlays showing the locations of the fields in which [C II] was observed with SOFIA for NGC 891 (left) and NGC 5907 (right) on visible-light images (A. Block, Mt. Lemmon SkyCenter Schulman telescope, wikimedia commons). The green boxes show the on-source coverage with SOFIA, and the yellow polygon outlines the region observed by *Herschel*. Labeled red rectangles show the strips from which vertical profiles were extracted in Fig. 3. Scale bars indicating ± 1 kpc ($52''$ for NGC 891 and $27''$ for NGC 5907) are shown for reference.

Archival, fully reduced, [C II] line integral images of NGC 891, part of the *Herschel* Very Nearby Galaxies Survey (Hughes et al. 2015), were analyzed to generate a vertical profile for the inner galaxy at 1–2 kpc galactocentric radii. Inspecting Fig. 5 from Hughes et al. (2015), there was already a hint of a change in the slope of surface brightness versus altitude, indicating an extraplanar gas component distinct from gas in the disk of NGC 891. The *Herschel* observations were unchopped and had to be corrected for transients (Fadda et al. 2016). Comparing the *Herschel* and

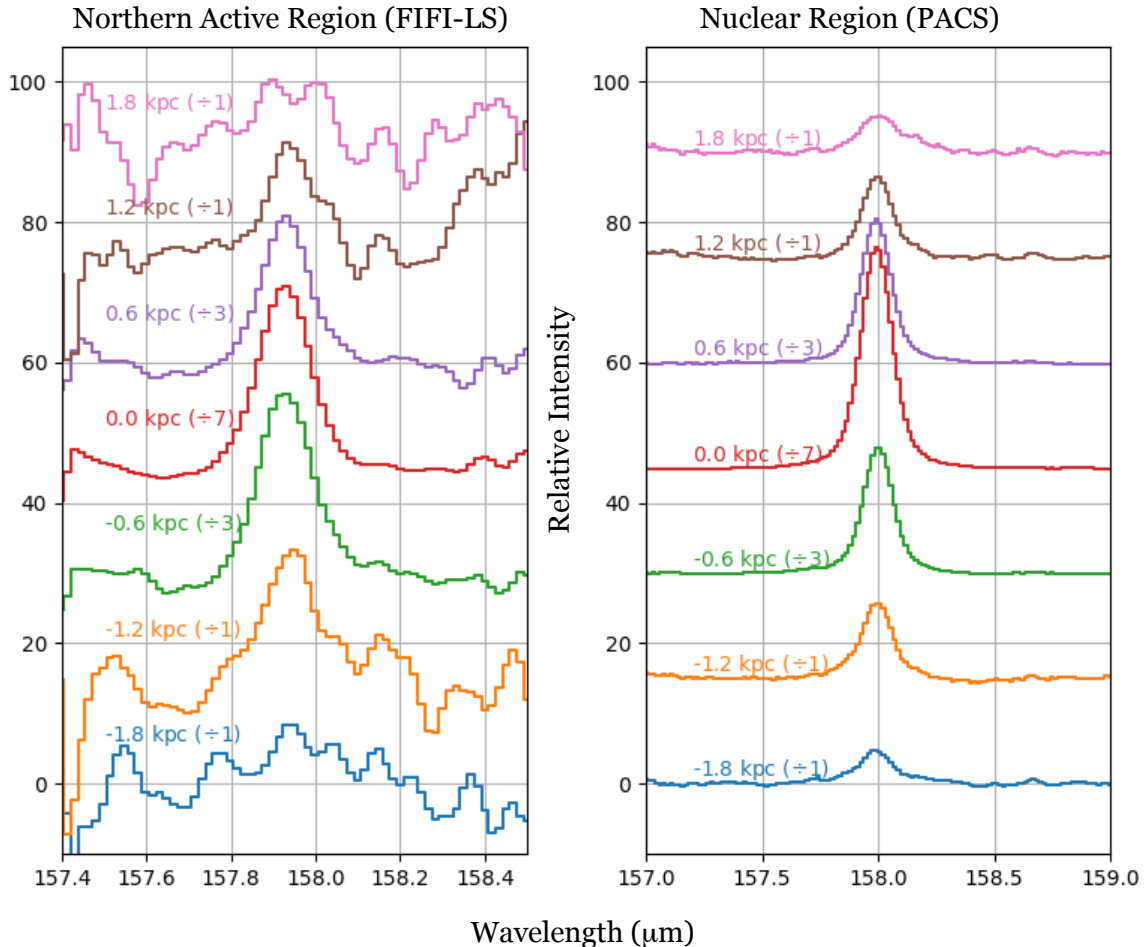


Figure 2. Spectra of NGC 891 observed by SOFIA in the northern disk (left panel; A & B in Fig. 1) and by *Herschel* (right panel; N in Fig. 1) through the nucleus in the [C II] 157.741 μm line. The spectra are averaged over longitudes in the NGC891-North map, at each of 7 labeled distances (in kpc) from the midplane. The spectra divided by scale factors (labeled) to better fit onto the diagram.

SOFIA observations in detail shows a potentially steeper decline of [C II] in the *Herschel* data from 0–1 kpc. Only a small part of this difference is the slightly larger SOFIA beam.

To verify the calibration and quality of the SOFIA/FIFI-LS data, we extracted the spectrum of a portion of the NGC 891 disk (the southernmost portion of the disk in the NGC 891-North field) that was observed with *Herschel*/PACS. We used the same spatial aperture and spectral baseline to extract the spectrum. The in-aperture flux measured with FIFI-LS was $(2.78 \pm 0.09) \times 10^{-15} \text{ W m}^{-2}$, while that measured with PACS was $(2.76 \pm 0.01) \times 10^{-15} \text{ W m}^{-2}$, in excellent agreement. To check the effect of using the FIFI-LS spectral baseline, we used a wider baseline in the PACS spectrum to find a flux 4% higher. A $\sim 4\%$ uncertainty in flux due to bandpass differences between FIFI-LS and PACS have negligible effect on the analysis in this paper.

3. RESULTS

3.1. NGC 891

Figure 2 shows the averaged [C II] spectra at 5 different altitudes, z , above the midplane, where the $+z$ direction is toward celestial northwest. Each spectrum was averaged over longitudes covering the bright midplane H II regions in the Northern NGC 891-North field (see Fig. 1), and each spectrum includes a 1-beam (0.6 kpc) strip of altitudes centered on the labeled altitude. The midplane spectra are detected with a signal-to-noise of approximately 40 per wavelength resolution element. The spectra at ± 1.2 kpc clearly detect the [C II] line.

Table 2. Scale Height Fits

	NGC 891-N, starburst, -z	NGC 891-center	NGC 891-S	NGC 5907
resolution ^a (kpc)	0.32	0.20	0.32	0.63
scale height (kpc): thinner	0.40 ± 0.1	0.5 ± 0.1	0.3 ± 0.08	0.37 ± 0.05
scale height (kpc): thick	2.8 ± 0.7	2.8 ± 0.7	...	~ 3

^aHalf-width at half-maximum. Observed with SOFIA except NGC891-center, with *Herschel*

Figure 3 shows the derived vertical distribution of [C II] for NGC 891 at 7 different longitudes, at altitudes separated by approximately 1 beam. For NGC 891-N, we estimated the signal-to-noise at each z from the fluctuations in the longitude-averaged spectra within the spectral baseline windows. The midplane [C II] flux is detected with signal-to-noise greater than 100, and the flux at ± 1 kpc is detected with signal-to-noise greater than 10. The flux at ± 2 kpc remains above the detection limit with signal-to-noise approximately 4, but the signal is not detected beyond 2.4 kpc from the midplane.

To quantify the vertical extent of the [C II] emission, we compare the observed vertical profiles to those expected for exponential disks, $I \propto \exp(-|z|/H)$, convolved with the angular resolution of SOFIA/FIFI-LS (16'') or *Herschel*/PACS (10''). We first fit a single-scale-height model, which was adequate for the NGC 891-S profile. Then we fit a two-scale-height model for the NGC 891-N and nuclear profiles. The two-scale-height model includes coupled (partially degenerate) parameters and is not a unique solution; in particular, the second scale height is not tightly constrained due to lack of signal-to-noise at the highest z . The convolved models are shown in Fig. 3 as dashed lines and reasonably well describe the overall trend. The model scale heights are summarized in Table 2. The discrepancies between model and observed profiles are partly due to real structure in longitude (discussed below). *bfc orientation* Furthermore, the northern and southern profiles are different, as can be seen in Fig. 3, indicating asymmetry in the origin of the extraplanar material.

At low altitudes from the NGC 891 midplane, the brightness is primarily from a thin disk with scale height in the range 0.25–0.4 kpc. It is thickest on the northern field, where there are giant H II regions in the midplane, and thinner in the more-quiet southern field. For the active starburst portions of the northern field (in the $-z$ direction) and the central part of the galaxy (both directions), a second component with scale height around 2.8 kpc is required. This wider component contributes only 3% of the [C II] model brightness in the midplane (before convolution with the PSF), but with its larger scale height it contributes 22% of the total brightness integrated over z and most of the brightness for lines of sight above 1.2 kpc from the midplane.

3.2. NGC 5907

Figure 4 shows the averaged [C II] spectra at 7 different altitudes for NGC 5907, with the $+z$ direction is toward celestial northeast. In NGC 5907, the width of the [C II] is much greater than an unresolved disk, despite the lower physical resolution of the observations compared to NGC 891 (due to the greater distance of NGC 5907). Figure 4 shows clear detections of [C II] out to 1.8 kpc from the midplane. Figure 5 shows the vertical profile compared to the convolved exponential disk model as used in the previous subsection. The illustrated model does not match the data particularly well. It does, however, show that the vertical distributions on the two sides ($+z$ and $-z$) of the midplane are different, with the galaxy somewhat thicker in the $-z$ direction near the midplane, but having a longer ‘tail’ to higher z in the $+z$ direction. The SOFIA observations detect the extended extraplanar gas up to 1.8 kpc from the midplane in both directions.

The measured scale heights of the galaxies are somewhat larger than the true scale heights, because the galaxies are not seen completely edge-on. To estimate this effect for NGC 5907, we modeled a tilted disk that is exponential in galactocentric radius and absolute vertical extent, then compared the profiles at a range of inclinations. For $i = 90^\circ$, perfectly edge-on, the observed vertical profile is the same as the projected. As i decreases, the predicted profile for the double exponential disk model is closely matched by a smoothed version of the true vertical profile. If the radial exponential scale length is H , then to a reasonable approximation, the observed vertical tilted profile is the true vertical profile smoothed by $16 H \cos i$. For NGC 5907, at $i = 86.5^\circ$ (Garcia-Burillo et al. 1997), the observed profile

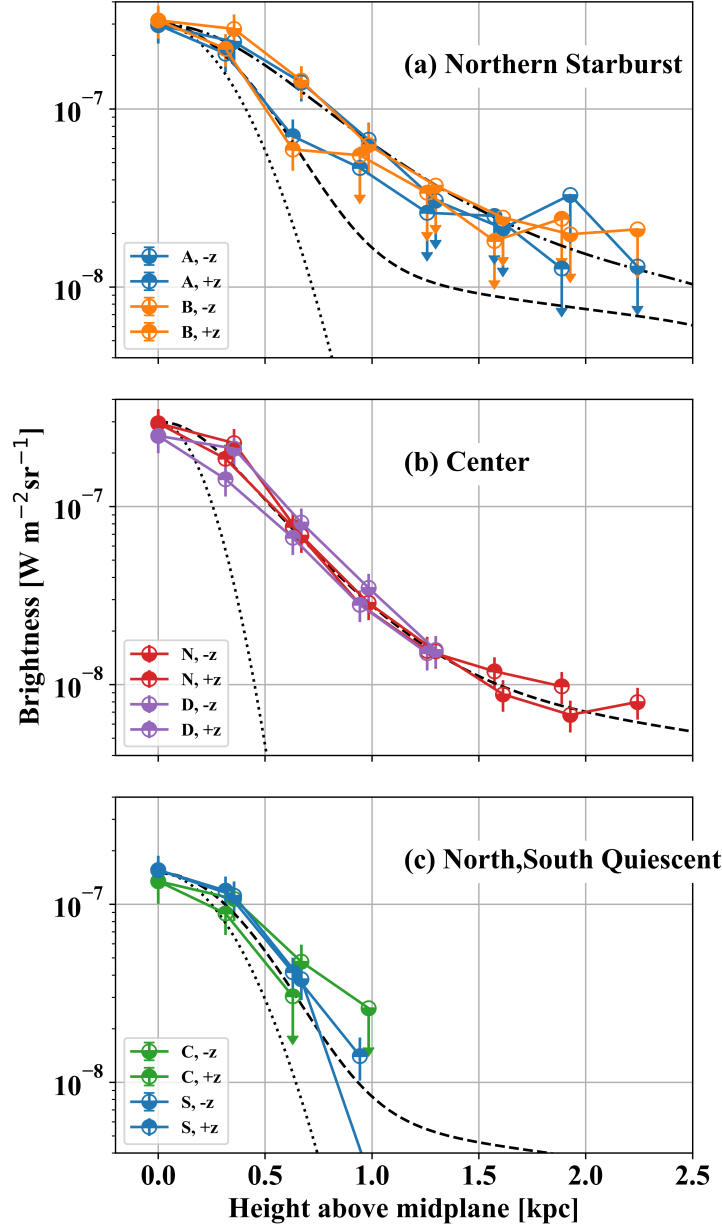


Figure 3. Vertical profiles of [C II] in NGC 891, showing the line brightness versus height above the midplane for slices through the galaxy at 7 different longitudes. The location of each slice through the galaxy is shown in Fig.1. The top panel (a) shows the vertical profile at two locations in the Northern field observed by SOFIA/FIFI-LS. The profiles for the $+z$ and $-z$ directions are shown separately, with symbols with the upper and lower halves, respectively, filled. The two longitudes in this panel cross through bright H II regions in the midplane. The center panel (b) shows profiles at through locations closer to the center of the galaxy observed by Herschel/PACS. The bottom panel (c) shows profiles for the southern field and a northern field observed by SOFIA/FIFI-LS where the star formation activity in the midplane is lower than in panel (a). In each panel, the black dotted line shows the observatory point spread function (PSF), normalized to the midplane brightness. Also in each panel, dashed black lines show exponential scale-height models (convolved with the PSF) described in the text and listed in Table 2. In panel (a), two such fits are shown, for the $-z$ (dashed-dot) and minimum fit to $+z$ (dashed) directions.

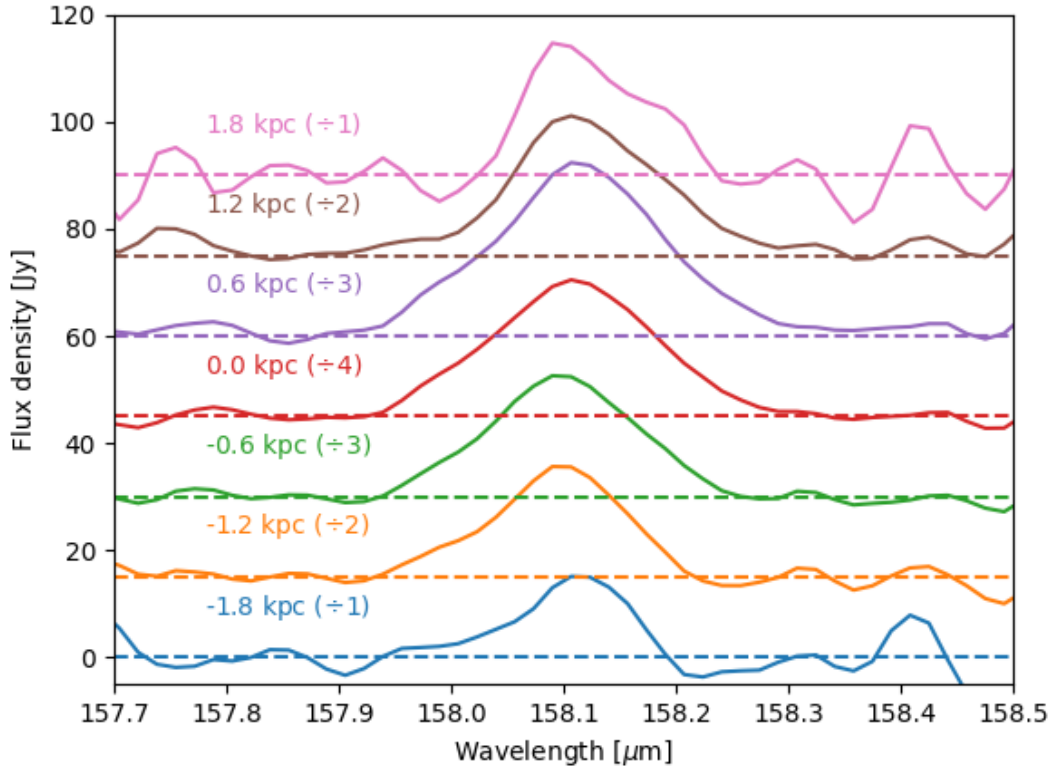


Figure 4. Spectra of NGC 5907 observed by SOFIA in the [C II] 157.741 μm line averaged over all longitudes observed, at each of 7 labeled distances (in kpc) from the midplane. The spectra divided by scale factors (labeled) to better fit onto the diagram.

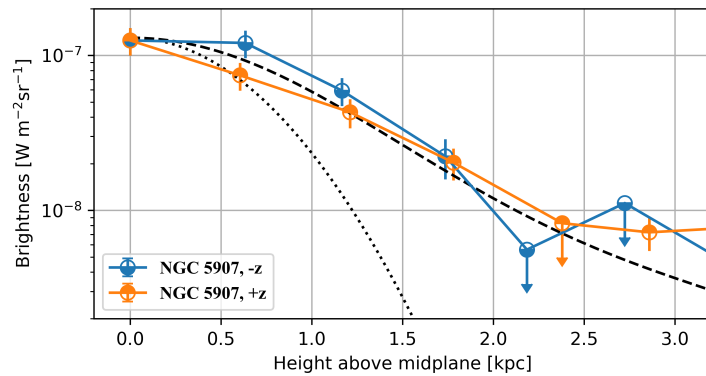


Figure 5. Vertical profiles of [C II] in NGC 5907, showing the line brightness versus height above the midplane for slices through the center of the galaxy. The profiles for the $+z$ and $-z$ directions are shown separately, with symbols with the upper and lower halves, respectively, filled. The black dotted line shows the observatory point spread function (PSF), normalized to the midplane brightness. The dashed black lines show an exponential scale-height models (convolved with the PSF) described in the text and listed in Table 2.

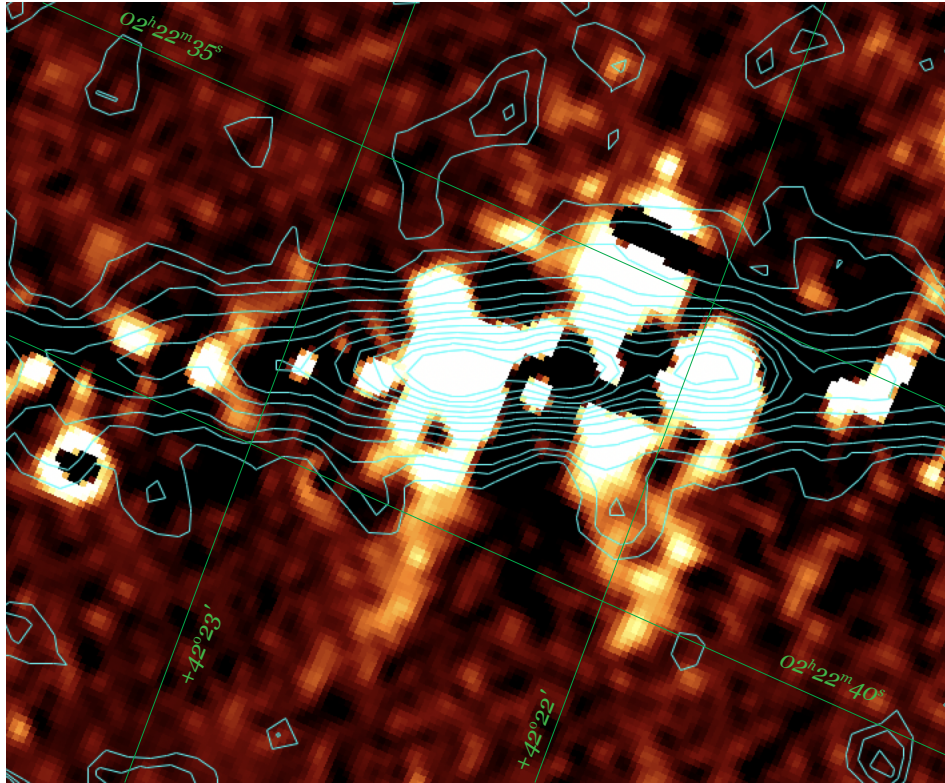


Figure 6. Overlay of SOFIA [C II] emission contours on the spatial-filtered H α image (from Rand et al. 1990). The region covered is shown in Fig. 1 as the northern box; it has been rotated counterclockwise so that the midplane is horizontal. The [C II] brightness is from a single channel at -200 km s^{-1} relative to the central velocity of the entire galaxy. The H α image shows the giant H II regions of the midplane (partially interrupted by extinction lanes), with prominent vertical extensions that correspond to [C II] features discussed in the text. The coordinate grid (J2000) is overlaid.

is the true one smoothed by $0.98 H$, so the true scale height is approximately $0.7/\sqrt{1+0.98^2} = 0.5 \text{ kpc}$. Note that this approximation only applies for smooth, exponential disk; some of the apparent vertical variation may be due to arms or far-outer-galaxy H II region (though this should make the profile very asymmetric which is not observed). (In comparison, for NGC 891, at $i > 89^\circ$ (Oosterloo et al. 2007), the true profile only needs to be smoothed by $0.28H$ or less, so the observed scale height is less than 4% larger than the true one.)

4. DISCUSSION

4.1. Relationship between extraplanar [C II] and Chimneys

The presence of metal-bearing material far from the midplane of the galaxies suggests a cycling of material such as in a galactic fountain, where massive star formation expels material from the midplane (Shapiro & Field 1976; Bregman 1980; Norman & Ikeuchi 1989). The extraplanar gas must be either maintained at its altitude by a significant pressure of underlying gas, or displaced from the midplane by transient events after which it returns to the midplane. Vertical extensions in edge-on galaxies have been interpreted as ‘chimneys’ through which massive star-forming regions vent material into the halo (Rand et al. 1990); such structures in the Milky Way have been labeled ‘worms’ (Heiles et al. 1996).

The new [C II] images show that ionized carbon also extends to the vertical heights of the chimneys at 2 kpc. Our view of the 2-dimensional distribution of the [C II] is limited by signal to noise, but for NGC 891 some reasonably well-defined structure is present. Figure 6 shows a direct overlay of the H α on the [C II] image. The H α image has already been spatially filtered to emphasize structure. Six giant H II regions in the midplane are evident, with the primary ones near the center of the imaged region. The region containing the H II regions is also prominent in [C II]. It is likely a combination of molecular clouds, massive stars and the interfaces between that are photodissociation regions, which are likely the source of most of the [C II] in NGC 891 (Stacey et al. 2010).

Extending vertically downward from the brightest H II regions in Figure 6 are two roughly vertical H α features. We will call them ‘chimneys’, for descriptive purposes. There are two prominent H α features, and both have associated [C II]. These features could conceivably be part of the same structure (i.e. limb-brightened walls of one chimney); however, that structure would be 2 kpc across and would likely be highly distorted by galactic shear in 60 Myr (if the rotational shear of NGC 891 is similar to that of the Milky Way). We will consider these structures to be two separate features, most likely related to the H II regions from which they appear to extend.

The H α plume extended downward from the midplane, just left of center in Fig. 6, has a somewhat diagonal [C II] feature that is centered in the base of the H α , filling in a location where the H α appears to have a void. This configuration could be caused by denser material near the midplane that remains relatively neutral (most of the H in atomic or molecular form) and also by extinction blocking the H α .

For the other prominent downward chimney, just right of center in Fig. 6, there is again a corresponding [C II] feature in the ‘base’. The base of this chimney is also evident in a *Hubble* image as a filament extending about 690 pc from the midplane (Fig. 8 of [Rossa et al. 2004](#)).

On the upward side of the midplane, there are no prominent H α chimneys in this part of the galaxy. The H α image shows one prominent vertical feature that lies just to the right of Fig. 6 (outside the area well-covered by SOFIA) and near the eastern edge of the PACS image, making it difficult to assess the correspondence.

With the present data, it cannot be unequivocally determined whether the [C II] and H α structures are physically related. However, the correspondence is strong enough that we explore the possible implications. The [C II] and H α lines can trace regions of different physical conditions and, most importantly, of different illumination by hot, ionizing stars in the midplane. The massive star forming clusters that may have ejected the material into the halo (or a previous generation in the same spiral arm) send ionizing photons on straight sightlines wherever they avoid intercepting optically thick clouds. Regions that are behind an H column density greater than 10^{21} cm $^{-2}$ have enough intervening dust to be shielded from far-ultraviolet photons so the H is neutral. The chimneys will therefore have ‘walls’ that will not necessarily emit in H α . The [C II], then, traces the colder gas in the walls of the chimneys.

Assuming the [C II] line emission arises from neutral gas, we use the observed surface brightness of 1.9×10^{-4} erg cm 2 s $^{-1}$ sr $^{-1}$ to derive the neutral gas column density. Using line cooling rate from [Goldsmith et al. \(2012\)](#) and carbon abundance from [Cardelli et al. \(1996\)](#), the observed [C II] requires a significant column density, of order

$$N_{\text{H}} \simeq 4 \times 10^{22} f(T)^{-\frac{1}{2}} \left(\frac{L}{100 \text{ pc}} \right)^{\frac{1}{2}} \text{ cm}^{-2} \quad (1)$$

where the emitting region is has a path length of 100 pc. Equivalently, this column density estimate applies if the emitting region has a volume density of 65 cm $^{-3}$, and it scales inversely with volume density. The temperature dependence is weak (unless the gas is very cold):

$$f(T) \equiv \exp^{-0.91 \left(\frac{100}{T} - 1 \right)} \left(\frac{T}{100} \right)^{0.14} \quad (2)$$

which has values $f(T) = 0.1, 0.4, 1, 1.9,$ and 2.6 at $T = 30, 50, 100,$ and 500 K, respectively. The high column density means that the [C II] emitting region is optically thick to UV and visible radiation. Ionization of C must be maintained by optically thin path lengths interior to the chimney walls, which then form a photodissociation region. Dust mixed with the ionized gas in the H α emitting interior of the chimney may provide some opacity, but the dust/gas ratio could be low due to dust destruction during the violent ejection of material from the midplane.

If, on the other had, the [C II] arises from ionized gas, and the emitting region has path length L , then the emission measure of ionized gas is

$$\text{EM} \equiv \int n_e^2 dL = 1.5 \times 10^3 \left(\frac{T}{10^4} \right)^{0.35} \text{ cm}^{-6} \text{ pc} \quad (3)$$

for the observed [C II] surface brightness and Milky Way metallicity ([Reynolds 1992](#)). The implied column density is significantly reduced (by a factor of ~ 40) if the gas is ionized, because excitation by electrons, much more abundant in fully ionized gas than in a PDR, is more efficient. Keeping the gas ionized requires a significant production of photons sufficiently energetic to ionize H. To balance the total recombination rate of the region, the ionizing photon production rate must be:

$$R_{\text{ion}} \sim 5 \times 10^{49} \left(\frac{L}{100 \text{ pc}} \right)^{\frac{1}{2}} \text{ s}^{-1}. \quad (4)$$

An ionization rate this high can be maintained if 2% of the ionizing photons from an open cluster of mass $10^5 M_\odot$ with largest star of $50 M_\odot$ escapes (Sternberg et al. 2003). The giant H II regions in the midplane underneath the H α chimneys may well be able to supply the needed ionizing photons. Observations of many giant H II regions in other galaxies have sufficient photon production even with 1% escape rates, as does W49 and NGC 3603 in the Milky Way, and 30 Dor in the LMC and N66 in the SMC (Kennicutt 1984). It thus appears plausible that the [C II] could arise from a large amount of neutral gas in PDRs in chimney walls, or from a smaller amount of gas kept fully ionized by ultraviolet photons leaking from the giant H II regions in the midplane.

The new observations presented here show some evidence for structure of the extraplanar gas, but with improved sensitivity the issue could be resolved and address the structure of the disk-halo interface in more detail. The *Herschel* observations of NGC 891 included a square map of the central portion of the galaxy and a strip along the midplane. The strip does not extend sufficiently to trace the extended gas. The square map of the central portion of NGC 891 extends to partially overlap about 15% of our NGC 891-North SOFIA field our observation, but due to its orientation, the overlap is primarily near the midplane, which does not allow for meaningful comparison or search for [C II] associated with chimneys apart from the inner portion of the galaxy. We see no clear evidence for [C II] structures associated with H α plumes that extend above and below the galaxy’s nucleus and above a giant H II region in the midplane north of the nucleus. Figure 7 shows the vertical profile for the central portion of NGC 891 (measured with *Herschel* together with the vertical profile for the northern portion of the disk (measured with SOFIA). The central portion of the galaxy images shows a steady decrease in [C II] with distance from the midplane indicating the cold, extraplanar gas above the inner portion of the galaxy is dominated by the thin disk, with a lower contribution from the thick disk.

4.2. Comparison of scale height with other tracers

Figure 7 compares the vertical profiles of various tracers of the ISM in NGC 891. The H I profile is from radio observations of the 21-cm line with the Westerbork Radio Synthesis Telescope (Oosterloo et al. 2007). The polycyclic aromatic hydrocarbon (PAH) profile was measured from archival mid-infrared observations with *Spitzer* in a broad waveband centered at $8 \mu\text{m}$ dominated by PAH emission. The same galactocentric radius range (3–7 kpc) as the SOFIA observation was extracted. The differences between the profiles show that they trace different phenomena. The widely distributed H I extends out to 100 kpc, with the inner portion potentially originating from a galactic fountain while the most distant gas is likely either primordial or stripped by gravitational interactions with other galaxies (Das et al. 2020). The thin disk in PAH emission that dominates the luminosity of the galaxy is due to present-day star formation (Smith et al. 2007). The molecular gas scale height traced by CO is 240 pc (Scoville et al. 1993; Yim et al. 2011), similar to the PAH, representing the reservoir of material forming stars.

The [C II] and H α trace both the thin star-formation disk and a ~ 2 kpc thick disk of extraplanar gas. Whether the thick disk relates to the extended H I is an open question. Low metallicity of the gas at 100 kpc argues against the most extended gas originating from the midplane, though the metallicity returns approximately to ‘normal’ within 5 kpc of the midplane (Qu et al. 2019). It therefore appears that the ~ 2 kpc disk we ascribe to the ‘chimneys’ or ‘galactic fountain’ is distinct from either the thin star-forming disk and the very extended H I.

The extraplanar distribution of [C II] for NGC 5907 is similar to that of H I (Table 2). Allaert et al. (2015) analyzed archival H I data and fitted it with a single scale height of 1.2 kpc.

4.3. Relationship between [C II] and Star Formation Tracers

The [C II] vertical distribution is far wider than the PAH emission (see Fig. 7). Both [C II] and PAH emission are associated with star formation in galaxies (Stacey et al. 2010). The PAH emission is likely to be more closely tied to star formation, because the PAH features are excited by absorption of UV photons that arise from early-type (hence, young) stars. The [C II] emission arises from many phases of the ISM including UV-heated star forming regions as well as diffuse interstellar gas heated by later-type (hence, older) stars. If we take the PAH emission as tracing the actual star formation rate (SFR), the extraplanar gas has a very different inferred [C II]/SFR ratio. In fact, at high z the PAH are excited and the C^+ is ionized by star-formation in the disk, so the local values of ‘SFR’ have relatively little meaning.

The difference in scale heights of [C II] emission and PAH indicate that the properties of the ISM and the dominant form of carbon changes from the disk to the halo of galaxies. The Milky Way average interstellar abundance (outside of molecular clouds) were derived by comparing the abundance of gas phase C^+ measured using *Hubble* to the interstellar C abundance of $\text{C}/\text{H}=2.4 \pm 10^{-4}$ derived from photospheres of B stars, and assuming all C is ionized but H is neutral

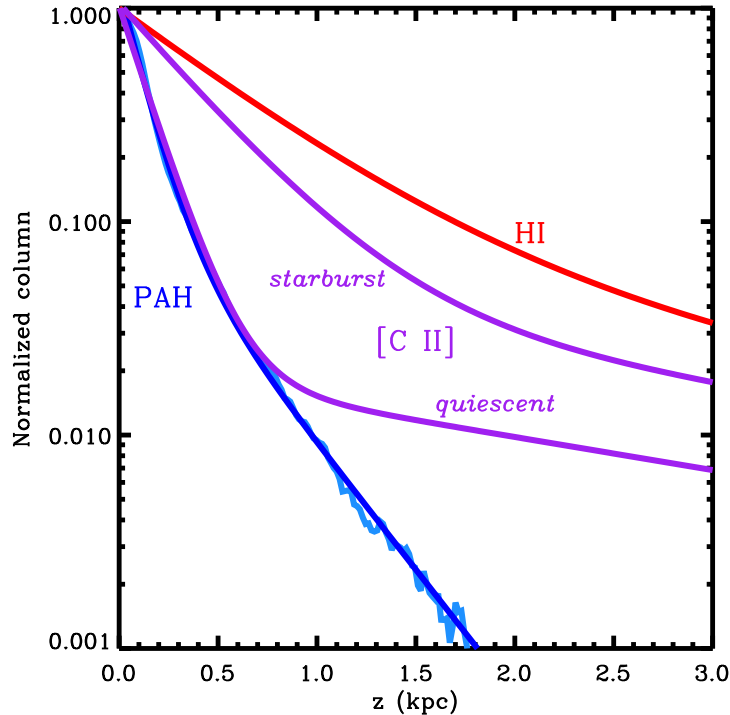


Figure 7. Vertical profiles of NGC 891. The H I (red; resolution 1.3 kpc) extends well beyond the edge of the figure and includes extensive circumgalactic gas likely due to interactions with nearby galaxies. The PAH (blue; resolution 0.2 kpc) emission arises closer to the midplane and traces the present location of massive star formation. The [C II] distribution (purple; resolution 0.7 kpc) is shown for the starburst and quiescent locations from Fig. 3. The quiescent profile is primarily consistent with the profile of present star formation, traced by PAH, while the more extended profile for the starburst (regions A+B labeled on the image in Fig. 1) has a more significant extended component.

along the observed lines of sight; this results in an estimated $58 \pm 15\%$ of carbon in the gas phase (Cardelli et al. 1996). From the brightness of mid-infrared features in the average spectrum of the Milky Way measured by *COBE*, Dwek et al. (1997) found $25 \pm 5\%$ of carbon is locked in the polycyclic aromatic hydrocarbons (PAH). Modeling the dust properties, Li & Draine (2001) also found 25% of C in grains, with 19% in small PAH and 6% in larger particles modeled as graphite.

If the [C II] emission arises from walls of chimneys, then the radiation field is likely harder and the dust properties different. Further, some of the [C II] emission may arise gas where the hydrogen is partially ionized, in the transition between the fully ionized interior and the likely neutral walls. Improved images of the extraplanar gas in tracers of neutral gas may allow to distinguish these components. With the new data presented here, the [C II]/H I ratio increases with distance from the midplane. Compared to the average value within 0.5 kpc of the midplane, [C II]/H I is about 2 times higher at 1 kpc and 3 times higher at 2 kpc.

5. CONCLUSIONS

Using SOFIA, we observed the 157.7 [C II] μm emission line for two nearby, edge-on galaxies to determine the vertical distribution of the emission with respect to the thin galactic disks. In both NGC 891 and NGC 5907, the [C II] distribution contains a thick disk with a scale height of ~ 2 kpc. The thick disks are intermediate between the very extended H I 21-cm halos of low-metallicity inter/circumgalactic gas and the thin disks that contain star-forming regions and molecular gas. There is some evidence for longitudinal structure in the thick disk. The extraplanar [C II] may arise in the walls of ‘chimneys’ that connect the galaxies’ disks to the halo, where material is driven upward by winds and supernova of massive star forming regions. The walls may be shielded material that has been ejected by the current giant H II regions or their predecessors.

ACKNOWLEDGMENTS

Based in part on observations made with the NASA/DLR Stratospheric Observatory for Infrared Astronomy (SOFIA). SOFIA is jointly operated by the Universities Space Research Association, Inc. (USRA), under NASA contract NNA17BF53C, and the Deutsches SOFIA Institut (DSI) under DLR contract 50 OK 0901 to the University of Stuttgart. EXES is supported by NASA agreement NNX13AI85A. Financial support for the observational and theoretical work in this paper was provided by NASA through award #06_0010 issued by USRA.

Facility: SOFIA

REFERENCES

- Allaert, F., Gentile, G., Baes, M., et al. 2015, *A&A*, 582, A18
- Bocchio, M., Bianchi, S., Hunt, L. K., & Schneider, R. 2016, *A&A*, 586, A8
- Boettcher, E., Gallagher, J. S., I., & Zweibel, E. G. 2019, *ApJ*, 885, 160
- Boomsma, R., Oosterloo, T. A., Fraternali, F., van der Hulst, J. M., & Sancisi, R. 2008, *A&A*, 490, 555
- Bregman, J. N. 1980, *ApJ*, 236, 577
- Breitschwerdt, D., & de Avillez, M. A. 2006, *A&A*, 452, L1
- Cardelli, J. A., Meyer, D. M., Jura, M., & Savage, B. D. 1996, *ApJ*, 467, 334
- Das, S., Sardone, A., Leroy, A. K., et al. 2020, arXiv e-prints, arXiv:2005.13684
- Dwek, E., Arendt, R. G., Fixsen, D. J., et al. 1997, *ApJ*, 475, 565
- Fadda, D., Jacobson, J. D., & Appleton, P. N. 2016, *A&A*, 594, A90
- Fischer, C., Beckmann, S., Bryant, A., et al. 2018, *Journal of Astronomical Instrumentation*, 7, 1840003
- Garcia-Burillo, S., Guélin, M., & Neininger, N. 1997, *A&A*, 319, 450
- Goldsmith, P. F., Langer, W. D., Pineda, J. L., & Velusamy, T. 2012, *ApJS*, 203, 13
- Grenier, I. A., Casandjian, J.-M., & Terrier, R. 2005, *Science*, 307, 1292
- Heald, G., Józsa, G., Serra, P., et al. 2011, *A&A*, 526, A118
- Heckman, T. M., Armus, L., & Miley, G. K. 1990, *ApJS*, 74, 833
- Heiles, C. 1990, *ApJ*, 354, 483
- Heiles, C., Reach, W. T., & Koo, B.-C. 1988, *ApJ*, 332, 313
- . 1996, *ApJ*, 466, 191
- Hawk, J. C., & Savage, B. D. 1999, *AJ*, 117, 2077
- Hughes, T. M., Foyle, K., Schirm, M. R. P., et al. 2015, *A&A*, 575, A17
- Kennicutt, R. C., J. 1984, *ApJ*, 287, 116
- Langer, W. D., Pineda, J. L., & Velusamy, T. 2014, *A&A*, 564, A101
- Leroy, A. K., Bolatto, A., Gordon, K., et al. 2011, *ApJ*, 737, 12
- Li, A., & Draine, B. T. 2001, *ApJ*, 554, 778
- Marasco, A., Fraternali, F., Heald, G., et al. 2019, *A&A*, 631, A50
- Martínez-Delgado, D., Peñarrubia, J., Gabany, R. J., et al. 2008, *ApJ*, 689, 184
- Norman, C. A., & Ikeuchi, S. 1989, *ApJ*, 345, 372
- Oosterloo, T., Fraternali, F., & Sancisi, R. 2007, *AJ*, 134, 1019
- Pineda, J. L., Fischer, C., Kapala, M., et al. 2018, *ApJL*, 869, L30
- Qu, Z., Bregman, J. N., & Hodges-Kluck, E. J. 2019, *ApJ*, 876, 101
- Rand, R. J. 1996, *ApJ*, 462, 712
- . 1997, *ApJ*, 474, 129
- . 2000, *ApJL*, 537, L13
- Rand, R. J., Kulkarni, S. R., & Hester, J. J. 1990, *ApJL*, 352, L1
- Reach, W. T., Heiles, C., & Bernard, J.-P. 2015, *ApJ*, 811, 118
- Reynolds, R. J. 1992, *ApJL*, 392, L35
- Rossa, J., & Dettmar, R. J. 2003, *A&A*, 406, 493
- Rossa, J., Dettmar, R.-J., Walterbos, R. A. M., & Norman, C. A. 2004, *AJ*, 128, 674
- Schmidt, P., Krause, M., Heesen, V., et al. 2019, *A&A*, 632, A12
- Scoville, N. Z., Thakkar, D., Carlstrom, J. E., & Sargent, A. I. 1993, *ApJL*, 404, L59
- Shapiro, P. R., & Field, G. B. 1976, *ApJ*, 205, 762
- Smith, J. D. T., Draine, B. T., Dale, D. A., et al. 2007, *ApJ*, 656, 770
- Stacey, G. J., Charmandaris, V., Boulanger, F., et al. 2010, *ApJ*, 721, 59
- Stacey, G. J., Geis, N., Genzel, R., et al. 1991, *ApJ*, 373, 423
- Sternberg, A., Hoffmann, T. L., & Pauldrach, A. W. A. 2003, *ApJ*, 599, 1333

Yim, K., Wong, T., Howk, J. C., & van der Hulst, J. M.
2011, AJ, 141, 48